

Numerical Study of Stream-wise and Span-wise Nanosecond DBD Plasma Actuators Effects on Supersonic Flow Separation

A. Nazarian Shahrabaki, R. Khoshkhoo[†] and M. Bazazzadeh

Faculty of Mechanical Engineering, Malek Ashtar University of Technology, Iran

[†]Corresponding Author Email: r.khoshkhoo@mut.ac.ir

(Received December 22, 2021; accepted February 20, 2022)

ABSTRACT

The current paper aimed to investigate the primary control mechanism of various Nanosecond Dielectric Barrier Discharge (NS-DBD) plasma actuators on the Shock Wave/Boundary Layer Interaction (SWBLI). For this purpose, the effects of the NS-DBD actuator have been investigated on an $M=2.8$ supersonic flow numerically. The Reynolds Averaged Navier-Stokes (RANS) equations and $\kappa - \omega$ SST turbulence model were used as the governing equations to simulate the supersonic flow characteristics. The numerical simulation of the baseline flow (without plasma actuator) was verified using an investigation on wall pressure distribution and the size of SWBLI. Then, NS-DBD phenomenological model based on the energy deposition model in accordance with experimental data was applied to the baseline simulation. Moreover, various stream-wise and span-wise NS-DBD plasma actuator models were used to investigate the actuator effects on the studied flow's low-density separation zone. Comparing the numerical results of the stream-wise and span-wise actuations revealed that both actuator types cause a momentum transferred to the flow, consequently decreasing the SWBLI region's size and the boundary layer's thickness. The results showed that the presence of the NS-DBD actuator increased the local temperature of flow over the insulated electrode. In this regard, a stream-wise NS-DBD actuator with a length of 90 mm upstream of the SWBLI increased the separation flow velocity by 33.7% and decreased the length of the separation region by 5 mm. Also, in this case, after 170 microseconds from the start of actuation, the size of SWBLI decreased by 4.2 mm. Therefore, it can be concluded that the stream-wise type of actuation was more effective in reducing the flow separation and SWBLI size than the span-wise type due to vortex generation into the inlet flow and suppressing the SWBLI region. The proposed NS-DBD actuators were mainly capable of applying the momentum to the boundary layer and reducing the velocity of separated flow in the SWBLI zone. The micro shock wave propagation through the flow associated with the NS-DBD discharge of the actuators can produce more effective high-speed flow control.

Keywords: Span-wise/Stream-wise actuation; Nanosecond DBD; Plasma actuator; Flow separation; Shock Wave/Boundary Layer Interaction.

1. INTRODUCTION

Shock Wave/Boundary Layer Interaction (SWBLI) is a common occurrence in the supersonic flow, because flow deflection and compression usually occur with the formation of a shock wave (Smits and Dussauge 2006; Whalen *et al.* 2020). The features of the SWBLI depend on the characteristics of the upstream flow, the Mach number, the shock angle, and the shock wave source. The shock may interact with a free shear layer, a free-stream turbulent flow, or a turbulent boundary layer (Shinde *et al.* 2020). Figure 1 shows a schematic of SWBLI, oblique shock waves, and flow separation region (Verma and Manisankar 2018).

SWBLIs occur in supersonic intakes associated with a high-speed air-breathing propulsion system and can

lead to an adverse pressure gradient in the boundary layer. Consequently, the interactions may cause flow separation, leading to reverse flow in the SWBLI, and decreased total pressure, resulting in unstart of the vehicle's intakes and significant performance loss. Hence, the SWBLI control for reducing in the separation region's length excited strong research interest (Pirozzoli and Grasso 2006). Flow control is classified into passive and active methods based on energy expenditure and controlled by command. Use of passive vortex generators (Saad *et al.* 2012; Panaras and Lu 2015), grooves/riblets by Smith *et al.* (2004) are among passive methods, and active strategies include boundary layer suction/blowing (Sarimurat and Dang 2012), variable geometry

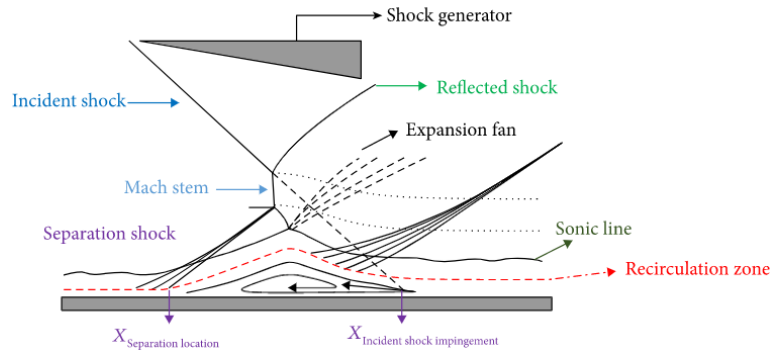


Fig. 1. Schematic of SWBLI in a supersonic flow.

systems (Falempin *et al.* 2006), and plasma actuators (Huang *et al.* 2020; Khoshkhoo and Jahangirian 2016).

In the last two decades, passive vortex generators have been widely used to mitigate the SWBLI size and the separation region (Lee *et al.* 2011). Vortex generators, such as micro-vanes and micro-ramps, reduce flow separation and alleviate SWBLI by transferring momentum to the boundary layer through stream-wise vortex generation. Although vortex generators have a simple structure and geometry, they reduce total pressure and generate aerodynamic drag. Most importantly, they are uncontrollable and must be used in off-design operation mode.

Nowadays, as a novel approach, plasma actuators can actively control the flow with high flexibility and controllability without additional aerodynamic drag. In recent years, plasma actuators have been recognized as an effective means of mitigating SWBLIs (Kinefuchi *et al.* 2018). Dielectric Barrier Discharge (DBD) plasma actuators are classified within non-thermal electro-hydrodynamic approaches (Mishra and Panigrahi 2020; Taleghani *et al.* 2018). Since excitation in DBD actuators is due to sinusoidal alternating input current, they are referred to as Alternating Current DBD (AC-DBD) plasma. They generate wall jet/body force near the plasma region, and consequently add momentum to the boundary layer flow.

The use of AC-DBDs has been widely considered in many research studies. The results of studies indicated that AC-DBDs could reduce flow separation at low speed and Reynolds number (Wei *et al.* 2019; Chen *et al.* 2020). The extremely low speed of the flow induced by AC-DBD actuators (it is several meters per second) makes them ineffective for use in supersonic flow, significantly to reduce the SWBLI size and flow separation. As another type, DBD actuators excited with nanosecond direct pulses, which are recognized as Nanosecond DBD (NS-DBD) plasma, have recently attracted scientists' attention in the subject of supersonic flow control.

Figure 2 shows an NS-DBD actuator and its components. According to the figure, after applying

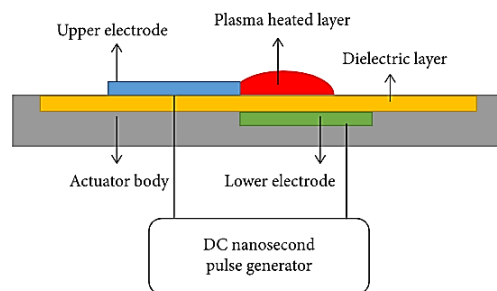


Fig. 2. Schematic view of an NS-DBD actuator.

a nanosecond DC pulse, the actuator produces a high-temperature region within few microseconds. Therefore, energy deposition is the primary mechanism by which NS-DBD actuators control SWBLI. The NS-DBDs instantaneously increase the flow temperature and pressure, and generate compressive waves around the discharge region (Wilde *et al.* 2021).

The NS-SDBD plasma actuator has two types of control mechanisms for control of SWBLI; boundary layer heating and vortex generation near the plasma surface. Boundary layer heating increases the separation bubble size, consequently, making SWBLI stronger. However, vortex generation is more capable of overcoming the boundary layer separation (Wilde *et al.* 2021).

The detailed control mechanism of NS-DBDs in high-speed flow like SWBLI mitigation needs to be better understood. Therefore, developing a numerical-based model is essential to recognizing the unknowns of SWBLI control using DBDs and their control mechanisms.

The characteristics of NS-SDBD actuators have been experimentally and numerically investigated in the following. The majority of studies on NS-DBD application are related to subsonic flow applications and quiescent flow (Znamenskaya *et al.* 2020; Kolbakir *et al.* 2020; Anzalotta *et al.* 2020; Zheng *et al.* 2014; Veerakumar *et al.* 2020). Therefore, limited studies have investigated SWBLI control in a supersonic flow regime.

The effect of NS-DBD actuators was investigated on a high-speed flow (Mach=2) by Webb (2010). Based on their results, thermal actuation with the aid of a plasma actuator decreased the separation region and shifted the reflected shock upstream by 4 mm. Falempin *et al.* (2015) investigated the effect of DBD plasma on controlling the location of normal shock in a supersonic intake (M=2-3) in the off-design operation mode. Plasma actuation in various operation modes had a significant effect on the structure of shock waves formation. Moreover, their results reveal that the plasma actuator with a power of 8.1 kW as the optimized output power, shifted the shock location to the upstream, and decreased the angle of the initial shock wave. Their results showed that adding a steady heat source to the SWBLI moved the separation shock upstream and increased the separation bubble size.

Liao *et al.* (2020) investigated shock waves generated by an NS-DBD plasma actuator in a high-speed flow over a wedge. The results showed that the heat energy released by the actuator in the vortex zone was the primary mechanism of supersonic flow control. The research by Starikovskii *et al.* (2009) concluded that the heat gas layer generated by the NS-DBD region, occurring in less than one microsecond, was the main reason for exciting the supersonic flow and, consequently, transfer the momentum to the boundary layer. Abdollahzadeh *et al.* (2014) used an energy deposition model to show the model's capabilities to capture the main features of the actuator effects correctly. In another study, Unfer and Boeuf (2009) developed a numerical model coupling the flow governing equations with an NS-DBD phenomenological model. They concluded that rapid localized heating in the boundary layer produced a microwave, similar to the experiment performed by Roupassov *et al.* (2009).

Some kinetic methods have been suggested to model the NS-DBD actuator effects (Orr *et al.* 2021; Chen *et al.* 2019). The kinetic approach requires computational cost and time; thus, simpler models have been suggested. In these models, classified in the phenomenological approaches, only the temperature profile generated by the actuator is considered. In this area, Gaitonde (2013) investigated the temperature distribution of an energy deposition model with a Gaussian profile and realized that the microwave released by the NS-DBD actuator had the

same features as the experiments conducted by Takashima *et al.* (2011).

The present paper aimed to explore the control mechanism of NS-DBD plasma actuators in a high-speed flow, especially in the SWBLI separation zone. As mentioned before, the level of NS-DBD plasma actuator effects is directly related to the actuator's electrodes configuration. Various electrode configurations result in vorticity generation and, consequently, momentum transferred to incoming flow or only heating to the flow and its consequences.

Previous studies on the NS-DBDs have focused on actuator modeling or applying NS-DBDs for low and high-speed and supersonic separation control. So, a numerical study of plasma discharge direction and examining the interaction of microwaves generated by NS-DBD and incoming flow is a novel subject. The novelty of this paper is using two types of plasma configurations to find out the primary mechanism of NS-DBD effects on the high-speed separation. Plasma electrodes parallel to the flow stream (called stream-wise) and vertical to the flow stream (called as span-wise type) were considered. We expected both configurations mentioned above to effectively generate vorticity into the incoming flow and suppress the SWBLI separation region. Hence, to conduct the investigation, a numerical code was applied using the NS-DBD phenomenological model (based on the energy deposition model) following optimal experimental data presented by Kinefuchi *et al.* (2017); (2018). Thus, a numerical code of the baseline flow without plasma actuator was verified by wall pressure distribution around the SWBLI and the size of SWBLI. Then, two NS-DBD configurations were applied with the numerical code to examine the actuator's effects on the studied flow's low-density vortex zone.

2. COMPUTATIONAL METHOD

2.1 Computational Domain and Governing Equations

Figure 3 shows the present study's computational domain and the NS-DBD plasma actuator's configurations. As presented in Fig. 3, a shock generator ramp was positioned at 14° to the x-axis. According to the experiment by Kinefuchi *et al.* (2018), the channel width, height, and length were set

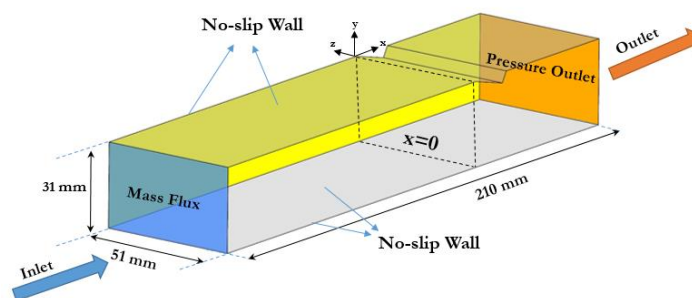


Fig. 3. Schematic view of computation domain.

to 51 mm, 30 mm, and 160 mm, respectively. The $x=0$ position was precisely set to the shock generator's start point. The inlet boundary condition was defined as the mass flux of $68 \text{ kg}/(\text{s}\cdot\text{m}^2)$ with a total temperature of 290 K. Considering the experimental tests by Kinefuchi *et al.* (2018), the thickness of the boundary layer exactly upstream of the separation region was approximately 4 mm. To match the numerical solution with the experimental results, a User Defined Function (UDF) was used to make the boundary layer thickness at the inlet plane of the channel equal to 2 mm. Considering the 2 mm boundary layer at the inlet plan of the channel has caused the numerical solution to be consistent with the experiment. Moreover, the boundary conditions of "pressure outlet" and "no-slip" are used to the outlet plan and all the walls of the channel, respectively.

A Mach 2.8 supersonic flow was numerically simulated, and the effects of NS-DBD actuations were investigated on the SWBLI. The governing equations are as follows, and details are presented by Wilcox (2006).

$$\frac{\partial \rho}{\partial t} + \frac{\partial(\rho u_j)}{\partial x_j} = 0 \quad (1)$$

$$\frac{\partial(\rho u_i)}{\partial t} + \frac{\partial(\rho u_i u_j)}{\partial x_j} + \frac{\partial p}{\partial x_i} - \frac{\partial \sigma_{ij}}{\partial x_j} = 0 \quad (2)$$

$$\frac{\partial(\rho e)}{\partial t} + \frac{\partial((\rho e + p)u_j)}{\partial x_j} - \frac{\partial(\sigma_{ij}u_i)}{\partial x_j} + \frac{\partial p}{\partial x_i} = Q \quad (3)$$

Where ρ is the density, t is the time, x_j is the position, u is the velocity, p is the flow pressure, σ_{ij} is the shear stress tensor, and Q is energy injected by the actuator (Duraisamy *et al.* 2019).

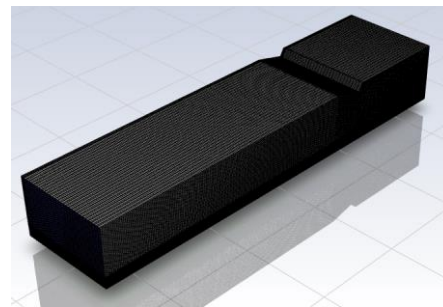
A Density-based solver is used to solve the above-mentioned unsteady equations with the time-step of 10^{-6} seconds. Discretization of these equations is done using second-order schemes. Besides, the residual acceptance levels for the momentum and energy equations are set to be less than 10^{-3} and 10^{-6} , respectively, as the convergence criteria of the numerical simulation.

2.2 Grid Specifications

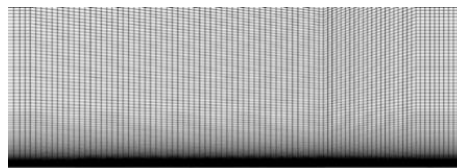
To perform the numerical grid study, simulations were conducted for different numbers of cells, as shown in Table 1. The figure compares the maximum

and average pressure for various grids with some different numbers elements. The table data shows that when the number of cells exceeded 4,200,000, the variation of numerical results is less than 0.5%. Therefore, the same number of cells was used to perform the simulations. Figure 4 demonstrates the structured mesh as the computational grid used in the present study. A finer mesh was used to increase the accuracy of the numerical results close to the separation zone.

The computational grid applied to the numerical solution domain is shown in Fig. 4. To increase the accuracy of the numerical simulation, the computational grid on the bottom wall is fine-tuned.



a) Computational domain



b) Finer mesh near the wall in the SWBLI region

Fig. 4. Applied computational grid.

Since the $\kappa - \omega$ SST turbulence model was used in numerical simulation, the Y^+ value distribution for the cross-section perpendicular to the channel and at the SWBLI region is shown in Fig. 5. It is noteworthy that the value of Y^+ in all areas of the computational domain is less than one, and near the lower level of the channel is estimated at 0.02. Also to meet the requirement of $Y^+ < 1$ in $\kappa - \omega$ SST turbulence model, the distance of the first layer from the bottom wall surface in the y -direction is equal to 1.2×10^{-7} meters.

Table 1. The results of the grid study.

Grid No.	No. of Cells	Max. Pressure (Pa)	Ave. Pressure (Pa)	Max. Pressure Difference (%)	Ave. Pressure Difference (%)
1	1,100,000	15,790	7,974	—	—
2	2,300,000	14,715	7,128	6.8	10.6
3	4,200,000	14,083	6,948	4.3	2.5
4	6,300,000	14,034	6,923	0.35	0.36

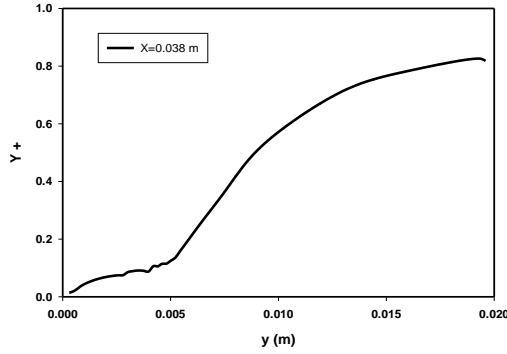


Fig. 5. Y^+ value distribution at plan $x=0.038$ m (in SWBLI region).

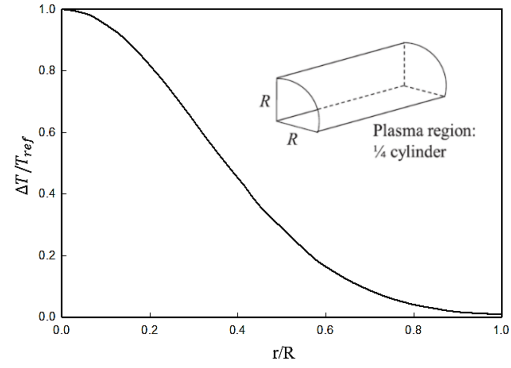


Fig. 6. Temperature rise distribution profile for NS-DBD plasma actuator.

2.3 Plasma Actuator Modeling

The plasma actuator was numerically simulated using a temperature profile and an energy deposition phenomenological model. Figure 6 shows the temperature profile applied to the plasma discharge region. According to Eq. (4), ΔT was applied to the plasma discharge region. It is assumed that the discharge region of NS-DBD is approximate a $\frac{1}{4}$ cylindrical shape with r radius. The temperature profile in the discharge region was radial and had a Gaussian profile (Gaitonde 2013) as Eq. (4).

$$\frac{\Delta T}{T_{ref}} = \exp\left[-n\left(\frac{r}{R}\right)^2\right] \quad (4)$$

The temperature rise inside the discharge region (ΔT) was associated with Q (amount of energy deposited) using the following equation:

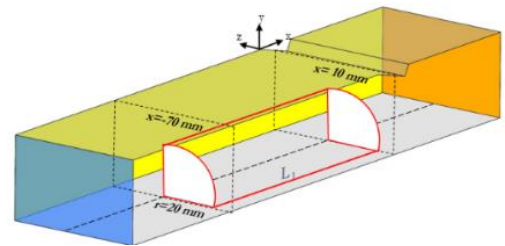
$$Q = \int \rho C_v \Delta T dV \quad (5)$$

where T_{ref} should be determined to satisfy Eq. (4), n is a constant and set to 5 to make a smooth distribution, r is the radial coordinate, R is the radius of discharge region, 20 mm, ρ is the air density, C_v is the specific heat coefficient, and dV is the volume element. Q is the amount of NS-DBD's energy, which is set to 50 mJ according to the experiment test by Kinefuchi *et al.* 2018.

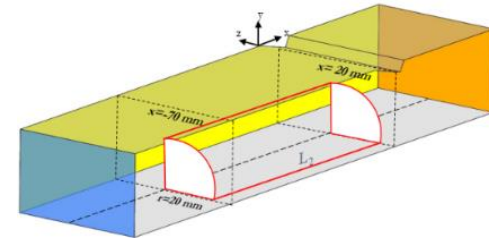
According to Eq. (4) and Eq. (5) and by considering the parameters mentioned above, the temperature rise distribution corresponding to the NS-DBD actuator in the $\frac{1}{4}$ cylindrical shape is presented in Fig. 6. According to the figure, the maximum temperature reached to position $r=0$ and the corner of the exposed electrode in the plasma actuator.

2.4 Configurations of Plasma Actuator

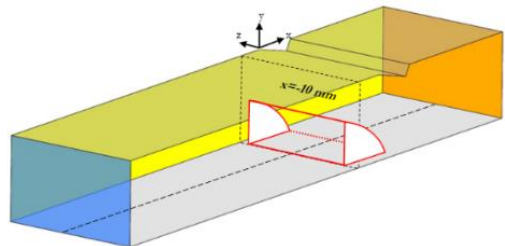
The configurations of stream-wise and span-wise NS-DBD plasma actuators are described in Fig. 7. In stream-wise type, electrodes were installed parallel to the flow direction, while in span-wise type, electrodes were installed vertically to the core-flow upstream of SWBLI. According to Figs. 7(a) and (b), various discharge lengths were considered to evaluate the plasma actuation effects: case 1 (with $L_1=80$ mm), and case 2 (with $L_2=90$ mm). In the first



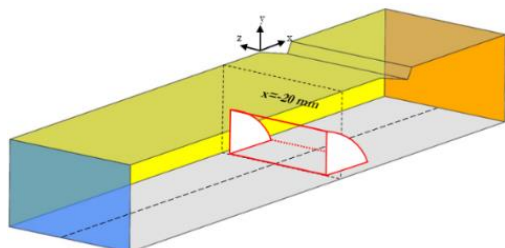
a) Test case of stream-wise plasma actuator, test case number 1



b) Test case of stream-wise plasma actuator, test case number 2



c) Test case of span-wise plasma actuator, test case number 3



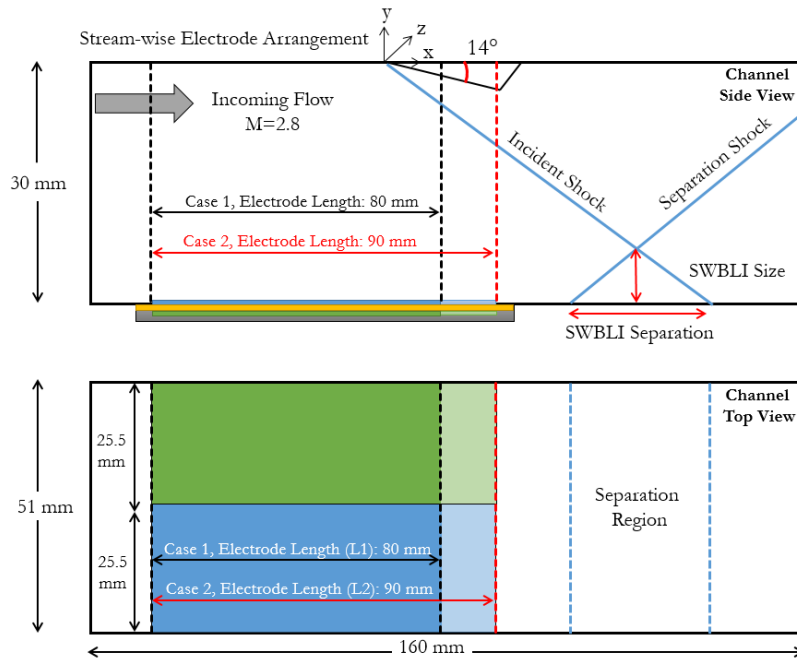
d) Test case of span-wise plasma actuator, test case number 4

Fig. 7. Spatial temperature distribution profile for NS-DBD plasma actuator.

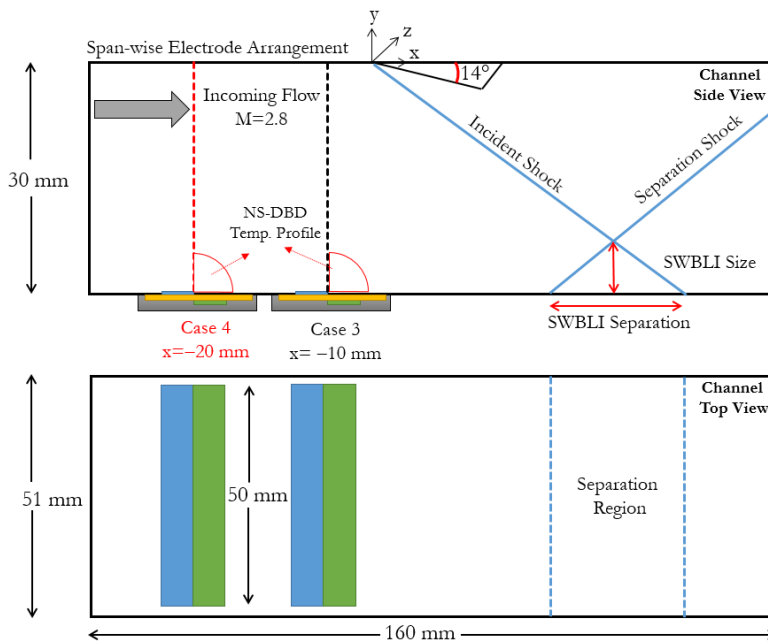
case, the actuator was limited to plane at $x=10$ mm, and in the second case, the actuator length was extended upstream of the separation at $x=20$ mm. Considering these simulation cases, we can evaluate the effect of energy deposition in parallel to the flow path and answer whether plasma actuation in the form of energy deposition, which extends closer to SWBLI, is efficient.

In span-wise type, two locations were considered for the energy deposition center. According to Fig. 7 (c) and (d), case 3 (at $x=-10$) and case 4 (at $x=-20$ mm) were considered to explore the plasma actuator location.

The four test cases revealed that the primary mechanism of NS-DBD in the desired flow regime was heating or vortex generating and that the micro shock wave was generated by NS-DBD. The detailed configurations of the test cases for both span-wise and stream-wise types are presented in Fig. 8. The figure also gives the solution domain, the coordination system, locations of actuators, and their dimensions. As shown in Fig. 8 (b), a distance of 0.5 mm is considered between the end of the plasma actuator and the channel wall to eliminate plasma discharge region/side walls interaction.



a) Test cases of stream-wise plasma actuator



b) Test cases of span-wise plasma actuator

Fig. 8. Schematic view of the computational domain and various plasma configurations.

3. RESULTS & DISCUSSION

3.1 Baseline Flow Field (Without Actuation)

To explore the verification of the numerical solution and flow field specifications around SWBLI, the baseline numerical simulation was compared with the experimental results data. Kinefuchi *et al.*'s (2018) study was used to ensure the accuracy of the simulation results. Figure 9 compares the flow pressure between the studied flow, including a different numbers of grids, and the experimental data by Kinefuchi *et al.* (2018). According to the figure, the numerical results by the grid, including 4,200,000 cells, match with the experimental results with an error of less than 1%.

Numerical results of the baseline solution around SWBLI are presented in Fig. 10. The results included the contours of the Mach number, stream-wise flow velocity, temperature, and pressure distribution at a plane in $Z=25.5$ mm.

The contour of flow density (dp/dx) variation generated by the numerical simulation at the middle plane of the domain is shown in Fig. 11 and was compared to the experiment (Kinefuchi *et al.* 2018). In both pictures, the angle of incident shock was 33.2° .

3.2 Plasma Actuation

As mentioned before, this study focused on two types of plasma discharge configuration as stream-wise and span-wise methods. For stream-wise type, two test cases were considered to investigate the effect of plasma discharge length on SWBLI as L_1 and L_2 . Two other test cases were used to explore the span-wise plasma actuation location on the separation region of SWBLI (X_1 and X_2). The detailed information on the test cases is presented in Table 2. Kinefuchi *et al.* (2017) studied the effects of actuation frequency variations on the size of SWBLI versus actuation time in the interval of 100 Hz to 10 kHz. Their results illustrate that the optimal actuation frequency is obtained at 2 kHz. Therefore, in this paper, the amount of NS-DBD energy deposition, temperature distribution, and the dimension of compression wave produced by the NS-DBD actuator are considered according to the optimal actuation frequency of 2 kHz (according to the results generated by Kinefuchi *et al.* (2017)).

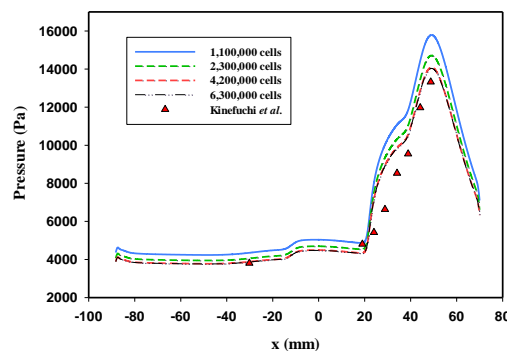


Fig. 9. Verification of numerical results.

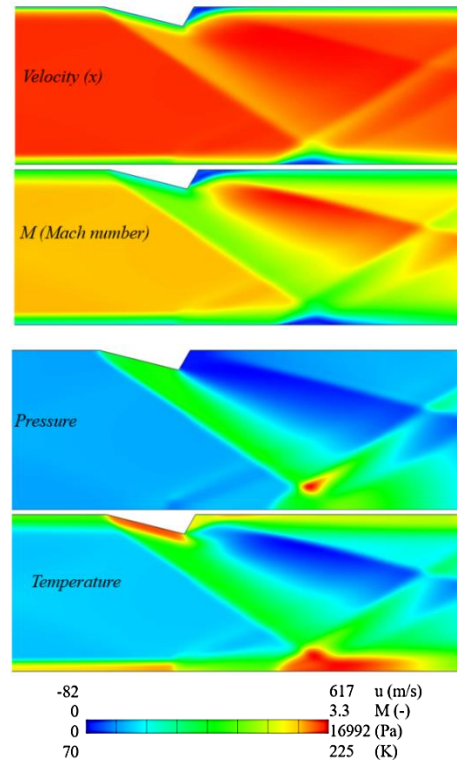


Fig. 10. Mach number, x-velocity, pressure, and temperature distribution of baseline flow.

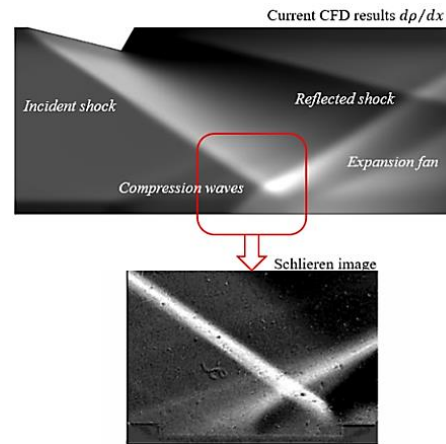
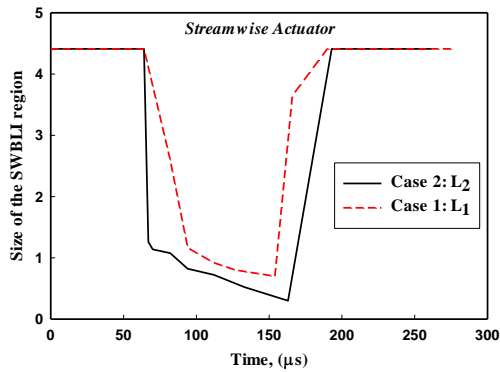


Fig. 11. Comparison of the numerical contour of dp/dx in SWBLI and experimental Schlieren image.

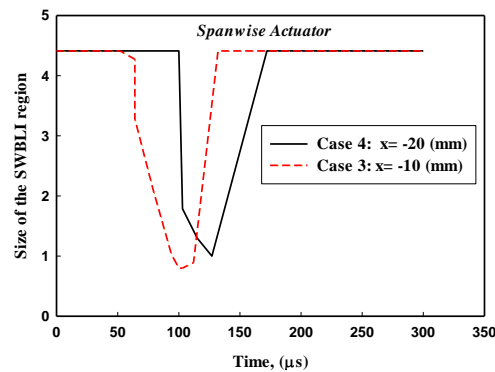
Table 2. NS-DBD plasma actuation types.

Case No.	Actuation Type	Parameter under investigation
1	Stream-wise	Actuator Length, $L_1=80$ mm
2	Stream-wise	Actuator Length, $L_2=90$ mm
3	Span-wise	Discharge Position, $X_1=-10$ mm
4	Span-wise	Discharge Position, $X_2=-20$ mm

Figure 12 shows the SWBLI region's size over actuation time for the test cases introduced in Table 2. In the figures, the start time of the NS-DBDs actuation was assumed from the beginning of the numerical simulation ($t=0$). Figure 12(a) shows SWBLI size variation for stream-wise type, and span-wise actuation results are presented as Fig. 12(b). Considering Fig. 8, the height between the intersection of the incident and reflected shocks, and the bottom wall is considered as the SWBLI size. It should be noted that SWBLI variation showed the movement of the reflected shock wave. The results showed that the SWBLI size was 4.4 mm when the actuator was off (baseline condition). Figure 12(a) indicates that the SWBLI size decreased at around 70 μ s after starting due to plasma actuation. It means that the reflected shock wave started to move upstream. After 95 μ s from plasma operation, the reflected shock wave returned to the primary state (4.4 mm) for both test cases. Comparison between L_1 and L_2 showed that the extended discharge length was slightly more efficient to reduce the SWBLI size.



a) Stream-wise plasma actuator



b) Span-wise plasma actuator

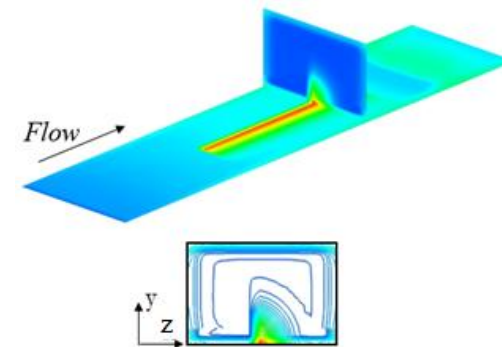
Fig. 12. Variation of SWBLI size over actuation time.

According to Fig. 12(b), the test cases with X_1 and X_2 were capable of reducing the SWBLI size. Each of the test cases reduced the SWBLI size according to its location. Therefore, the actuator and the induced microwave needed less time to affect the separation region by the closer location of the actuator to the SWBLI region. Also, the figures illustrated that the effect duration was longer on the flow in stream-wise

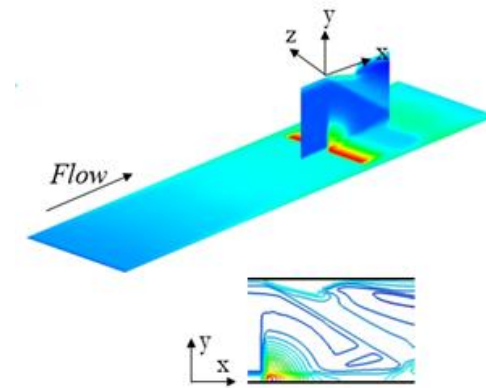
actuation than in span-wise actuation. The main reasons are the heating length and the period that the incoming flow interacts with the plasma discharge region. The more contact area of the incoming flow with the heated gas layer in the stream-wise type led the flow to have a more significant impact on the passing flow compared to the span-wise type. As mentioned before, it is concluded that the primary mechanism of both configurations was the generation of a momentum transferred to the core flow. Since the results of the test cases were similar to each other, the following simulation results were restricted to only one test case for each actuation type.

A) Temperature distribution of actuator:

In Fig. 13, the temperature distribution simulating the flow thermalization by NS-DBD actuator is presented for stream-wise and span-wise actuation types. The contours showed that the thermalization region complied with data illustrated in Fig. 6 ($1/4$ cylinder as plasma region).



a) Stream-wise actuation



b) Span-wise actuation

Fig. 13. Temperature distribution of NS-DBD plasma actuator at $t=0$ sec.

B) Pressure distribution:

The pressure development in the high-temperature region due to stream-wise actuation is described in Fig. 14. The data was extracted from a stream-wise plane located at $x=-10$ mm. The result showed that at $t=0$ sec, the pressure was proportional to the temperature profile as Fig. 13 (a). As noted in Fig. 14, the pressure rise on the top of the plane was due

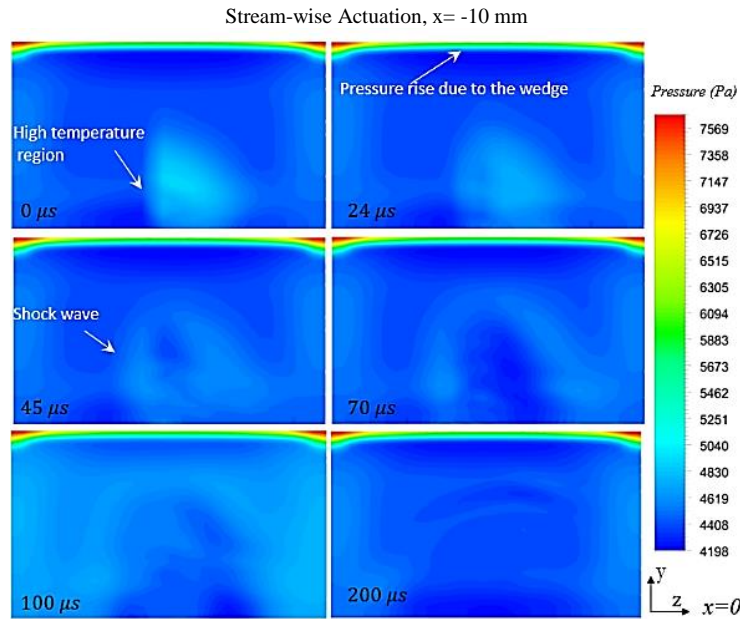


Fig. 14. Contour of pressure distribution around and upstream of SWBLI region in stream-wise actuation case.

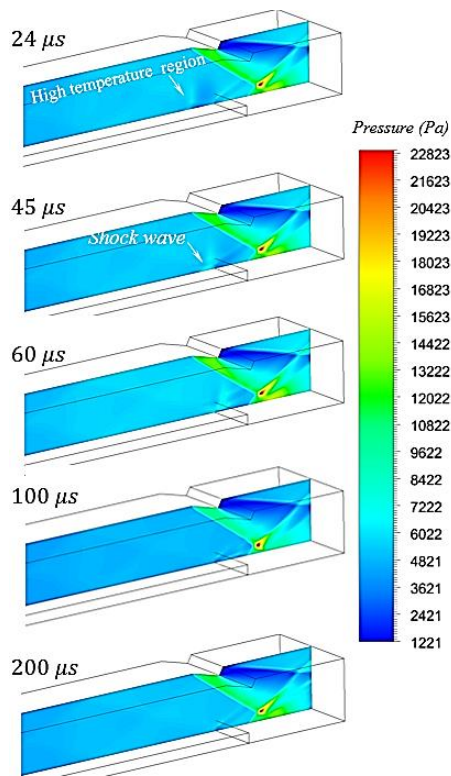


Fig. 15. Contour of pressure distribution in span-wise actuation case.

to pressure compression by the wedge. The microwave generated by the NS-DBD propagated in the plane at a velocity of 222 m/s in the y-direction. After 200 μ s from plasma discharge, the shock wave disappeared.

For the span-wise case, the pressure distribution of the plasma region is presented in Fig. 15. The numerical results illustrated that the compression

wave induced by the actuator propagated through the flow and met SWBLI after approximately 70 μ s.

C) X-direction velocity distribution:

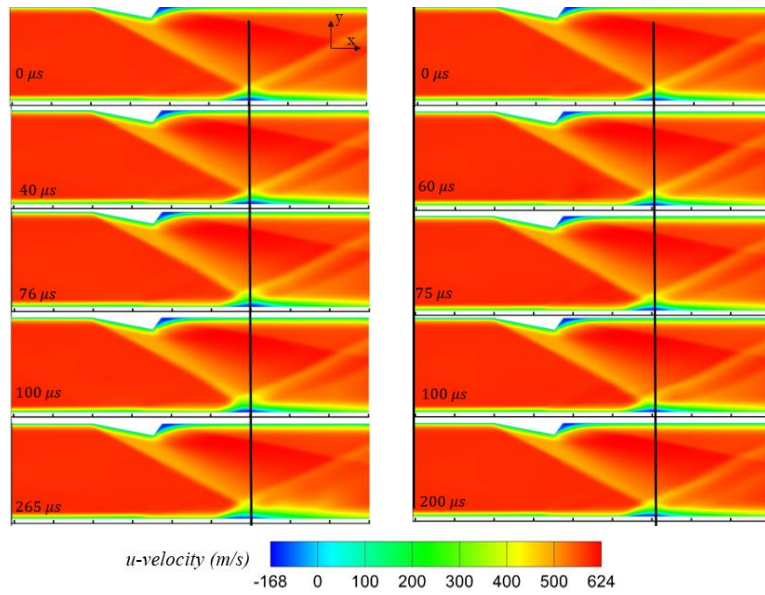
Figure 16 demonstrates the x-velocity distribution of stream-wise and span-wise cases. The separation area became small in both cases, as observed at $t = 200$ and 265μ s due to the induction of compression wave by the NS-DBD into the SWBLI region. The results of both cases illustrated that the plasma actuator produced a thin boundary layer using plasma shock wave propagation through SWBLI.

D) X-direction velocity profile

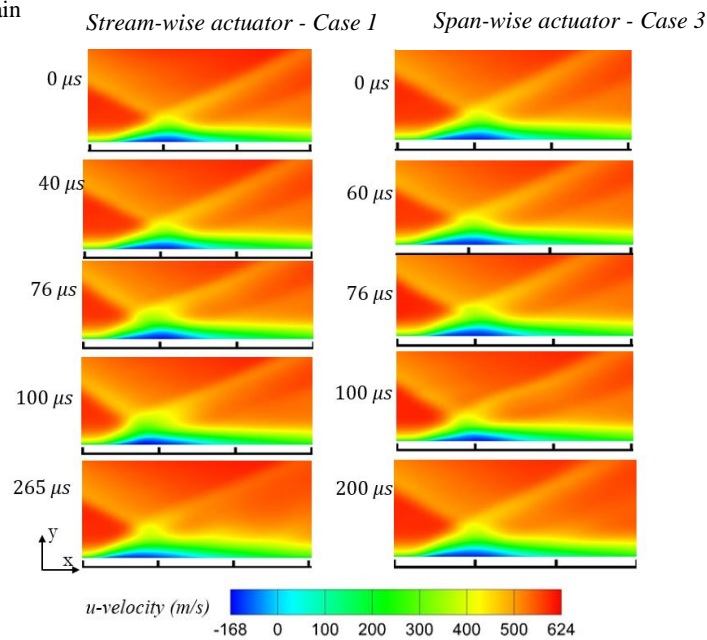
Figure 17 shows the variation of flow velocity at $x = 40$ mm (upstream of the SWBLI location at the discharge time of $t = 100$ microseconds). It was observed that acceleration of flow occurred in both stream-wise and span-wise actuation types. Comparing the results to the baseline velocity profile showed that stream-wise actuation could optimally reduce the backflow in the separation zone by applying the momentum to the flow.

According to Fig. 18, the separation area was affected by plasma actuation. The stream-wise simulation results presented in Fig. 18(a) showed that the separation length and reattachment point of separation decreased by plasma actuation. NS-DBD had the highest impact on separation control at 100 μ s.

The span-wise actuation results are described in Fig. 18(b). According to the figure, the compression wave released by the NS-DBD actuator met SWBLI approximately in $t=100 \mu$ s after plasma discharge. The most significant reduction occurred in the length of the separation region when the induced plasma shock wave passed SWBLI at times more than 190 μ s.

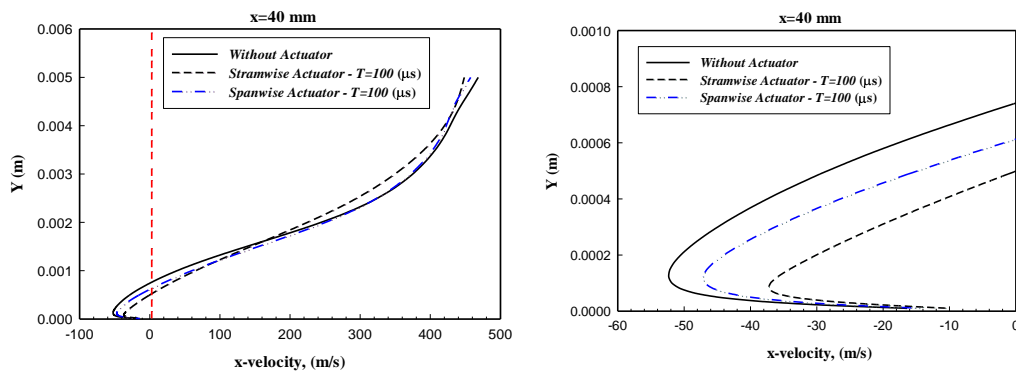


a) Full-scale domain



b) SWBLI region

Fig. 16. The contour of x-direction velocity distribution around and upstream of SWBLI region.



a) Full scale view

b) X-velocity profile in the separation region

Fig. 17. X-velocity profile in the boundary layer at $x = 40$ mm (upstream of the SWBLI at the discharge time of $t = 100 \mu\text{s}$).

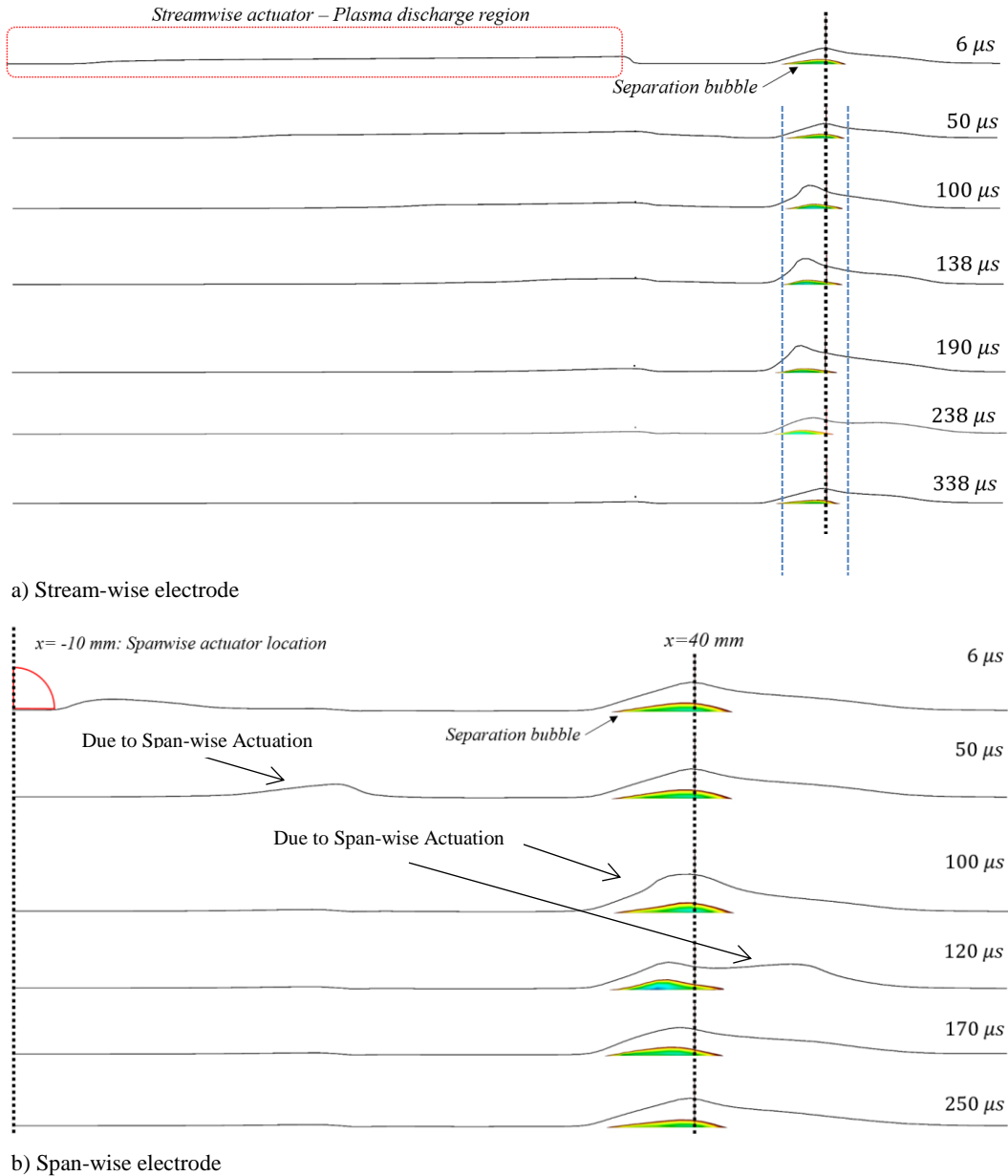


Fig. 18. Variation of separation region over actuation time.

1. CONCLUSION

The current study aimed at investigating the primary control mechanism of NS-DBD in high-speed flow. The effect of the NS-DBD plasma was directly related to the direction of the plasma actuation. The electrode configurations resulted in vortex generation and, momentum transfer to the boundary layer or flow heating. Stream- and span-wise applications of NS-DBD plasma actuators were investigated and analyzed in a Mach 2.8 numerically. For this purpose, 3D numerical analyses were performed for different actuation models. Plasma actuation with one burst/pulse was considered for numerical simulation. The results showed that in both stream- and span-wise cases,

the interaction of the compression wave released by the plasma actuator reduced the separation size.

For the stream-wise case, the plasma actuator with a length of 90 mm upstream of the separation region was more capable of reducing the SWBLI size. Therefore, it can be concluded that longer actuator length leads to a further time increases that affects the interaction size. Moreover, the simulations showed that the effective duration of the actuator on the flow was shorter in the span-wise case than in the stream-wise case. This value was estimated at about 70 μs for the span-wise case and about 100 μs for the stream-wise case.

Comparing the results of the stream- and span-wise cases revealed that both actuation cases generated a momentum force to the flow and,

consequently, decreased the SWBLI region's size. Moreover, plasma actuation reduced the boundary layer's thickness in both configurations. The proposed NS-DBD actuators were mainly capable of applying the momentum to the boundary layer, presented as an x-velocity profile upstream of SWBLI. Overall, microwave propagation through the flow due to the NS-DBD operation can result in the effective flow control.

REFERENCES

- Abdollahzadeh, M., J. C. Páscoa and P. J. Oliveira (2014). Two-dimensional numerical modeling of interaction of micro-shock wave generated by nanosecond plasma actuators and transonic flow. *Journal of Computational and Applied Mathematics* 270, 401–416.
- Anzalotta, C., K. Joshi, E. Fernandez and S. Bhattacharya (2020). Effect of forcing the tip-gap of a NACA0065 airfoil using plasma actuators: A proof-of-concept study. *Aerospace Science and Technology* 107, 106268.
- Chen, K., X. Geng, Z. Shi, K. Cheng and H. Cui (2020). Experimental investigation of influence of sliding discharge DBD plasma on low-speed boundary layer. *AIP Advances* 10, 35108
- Chen, T. Y., A. C. Rousso, S. Wu, B. M. Goldberg, H. Van Der Meiden, Y. Ju and E. Kolemen (2019). Time-resolved characterization of plasma properties in a CH₄/He nanosecond-pulsed dielectric barrier discharge. *Journal of Physics D: Applied Physics* 52, 18LT02.
- Duraisamy, K., G. Iaccarino and H. Xiao (2019). Turbulence modeling in the age of data. *Annual Review of Fluid Mechanics* 51, 357–377.
- Falempin, F., A. A. Firsov, D. A. Yarantsev, M. A. Goldfeld, K. Timofeev and S. B. Leonov (2015). Plasma control of shock wave configuration in off-design mode of M = 2 inlet. *Experiments in Fluids* 56(54).
- Falempin, F., E. Wendling, M. Goldfeld and A. Starov (2006). Experimental Investigation of Starting Process for a Variable Geometry Air Inlet operating from Mach 2 to Mach 8. In: *42nd AIAA/ASME/SAE/ASEE Joint Propulsion Conference & Exhibit*. American Institute of Aeronautics and Astronautics, California, USA.
- Gaitonde, D. V. (2013). Analysis of plasma-based flow control mechanisms through large-eddy simulations. *Computers & Fluids* 85, 19–26.
- Huang, J., B. Hu, Z. Li, J. Zhang, Z. Qian and S. Lan (2020). The Effects of Plasma-Based Body Force on Flow Separation Suppression. *Advances in Effective Flow Separation Control for Aircraft Drag Reduction. Modeling, Simulations and Experimentations*, Book Chapter, Springer International Publishing.
- Khoshkhoo, R. and A. Jahangirian (2016). Numerical Simulation of Flow Separation Control using Multiple DBD Plasma Actuators. *Journal of Applied Fluid Mechanics* 9(4), 1865-1875.
- Kinefuchi, K., A. Y. Starikovskiy and R. B. Miles (2017). Control of shock-wave/boundary-layer interaction using nanosecond-pulsed plasma actuators. *Journal of Propulsion and Power* 34, 909–919.
- Kinefuchi, K., A. Y. Starikovskiy and R. B. Miles (2018). Numerical investigation of nanosecond pulsed plasma actuators for control of shock-wave/boundary-layer separation. *Physics of Fluids* 30,106105.
- Kolbakir, C., H. Hu, Y. Liu and H. Hu (2020). An experimental study on different plasma actuator layouts for aircraft icing mitigation. *Aerospace Science and Technology* 107, 106325.
- Lee, S., E. Loth and H. Babinsky (2011). Normal shock boundary layer control with various vortex generator geometries. *Computers & Fluids* 49, 233–246.
- Liao, Y., I. V. Mursenkova, I. E. Ivanov, I. A. Znamenskaya and N. N. Sysoev (2020). Shock waves generated by a pulsed surface sliding discharge in a supersonic airflow past a wedge. *Physics of Fluids* 32, 106108.
- Mishra, B. K. and P. K. Panigrahi (2020). Flow field induced by a dielectric barrier discharge plasma actuator analyzed with bi-orthogonal decomposition. *Physics of Fluids* 32.
- Orr, K., X. Yang, C. Richards, E. Jans, S. Raskar, D. C. van den Bekerom and I. V. Adamovich (2021). Characterization and Kinetic Modeling of Ns Pulse and Hybrid Ns Pulse/RF Plasmas. In: *AIAA Scitech 2021 Forum*, P. 683.
- Panaras, A. G. and F. K. Lu (2015). Micro-vortex generators for shock wave/boundary layer interactions. *Progress in Aerospace Science*, Vol. 74, pp. 16–47.
- Pirozzoli, S. and F. Grasso (2006). Direct numerical simulation of impinging shock wave/turbulent boundary layer interaction at M=2.25. *Physics of Fluids* 18.
- Roupassov, D. V., Nikipelov, A. A., Nudnova, M. M., Starikovskii, A. Y. (2009). Flow separation control by plasma actuator with nanosecond pulsed-periodic discharge. *AIAA Journal* 47, 168–185.
- Saad, R., E. Erdem, L. Yang and K. Kontis (2012). Experimental Studies on Micro-ramps at Mach. *28th International Symposium on*

- Shock Waves*, Manchester UK, pp 861-866.
- Sarimurat, M. N. and T. Q. Dang (2012). Shock Management in Diverging Flow Passages by Blowing/Suction, Part 2: Applications. *Journal of Propulsion and Power* 28, 1230–1242.
- Shinde, V., J. McNamara and D. Gaitonde (2020). Control of transitional shock wave boundary layer interaction using structurally constrained surface morphing. *Aerospace Science Technology* 96, 105545.
- Smits, A. J. and J. P. Dussauge (2006). Turbulent shear layers in supersonic flow. *Springer Science & Business Media*.
- Smith, A. N., Babinsky, H. and Fulker, J. L. (2004). Ashill, P.R.: Shock Wave/ Boundary-Layer Interaction Control Using Streamwise Slots in Transonic Flows. *Journal of Aircraft* 41, 540–546.
- Starikovskii, A. Y., A. A. Nikipelov, M. M. Nudnova and D. V. Roupasov (2009). SDBD plasma actuator with nanosecond pulse-periodic discharge. *Plasma Sources Science and Technology* 18, 34015.
- Takashima, K., Y. Zuzeeq, W. R. Lempert and I. V. Adamovich (2011). Characterization of a surface dielectric barrier discharge plasma sustained by repetitive nanosecond pulses. *Plasma Sources Science and Technology* 20, 55009.
- Taleghani, A. S., A. Shadaram, M. Mirzaei and S. Abdolahipour (2018). Parametric study of a plasma actuator at unsteady actuation by measurements of the induced flow velocity for flow control. *Journal of the Brazilian Society of Mechanical Sciences and Engineering* 40(173).
- Unfer, T. and J. P. Boeuf (2009). Modelling of a nanosecond surface discharge actuator. *Journal of Physics D: Applied Physics* 42, 194017.
- Veerakumar, R., V. Raul, Y. Liu, X. Wang, L. Leifsson and H. Hu (2020). Metamodeling-based parametric optimization of DBD plasma actuation to suppress flow separation over a wind turbine airfoil model. *Acta Mechanica Sinica* 36, 260–274.
- Verma, S. B. and C. Manisankar (2018). Control of a Mach reflection-induced interaction using an array of vane-type vortex generators. *Shock Waves* 28, 815–828 .
- Webb, N. J. (2010). Control of Supersonic Mixed-Compression Inlets Using Localized Arc Filament Plasma Actuators. MSc. Thesis, The Ohio State University.
- Wei, B., Y. Wu, H. Liang, J. Chen, G. Zhao, M. Tian and H. Xu (2019). Performance and mechanism analysis of nanosecond pulsed surface dielectric barrier discharge based plasma deicer. *Phys. Fluids*. 31.
- Whalen, T. J., A. G. Schöneich, S. J. Laurence, B. T. Sullivan, D. J. Bodony, M. Freydin, E. H. Dowell and G. M. Buck (2020). Hypersonic fluid-structure interactions in compression corner shock wave boundary layer interaction. *AIAA Journal* 58, 4090–4105.
- Wilcox, D. C. (2006). *Turbulence Modeling for CFD*. DCW Industries.
- Wilde, N. D., H. Xu, N. Gomez-Vega and S. R. H. Barrett (2021). A model of surface dielectric barrier discharge power. *Applied Physics Letters* 118, 154102.
- Zheng, J. G., Z. J. Zhao, J. Li, Y. D. Cui and B. C. Khoo (2014). Numerical simulation of nanosecond pulsed dielectric barrier discharge actuator in a quiescent flow. *Physics of Fluids* 26.
- Znamenskaya, I., D. Tatarenkova, T. Kuli-zade and I. Ivanov (2020). Nanosecond discharges in a non-stationary flow around an obstacle. *Journal of Physics: Conference Series*. 12002.